
A Score-Based Model for Learning Neural Wavefunctions

Xuan Zhang

Computer Science and Engineering
Texas A&M University
College Station, TX 77843, USA
xuan.zhang@tamu.edu

Shenglong Xu

Physics and Astronomy
Texas A&M University
College Station, TX 77843, USA
slxu@tamu.edu

Shuiwang Ji

Computer Science and Engineering
Texas A&M University
College Station, TX 77843, USA
sj@tamu.edu

Abstract

Quantum Monte Carlo coupled with neural network wavefunctions has shown success in computing ground states of quantum many-body systems. Existing optimization approaches compute the energy by sampling local energy from an explicit probability distribution given by the wavefunction. In this work, we provide a new optimization framework for obtaining properties of quantum many-body ground states using score-based neural networks. Our new framework does not require explicit probability distribution and performs the sampling via Langevin dynamics. Our method is based on the key observation that the local energy is directly related to scores, defined as the gradient of the logarithmic wavefunction. Inspired by the score matching and diffusion Monte Carlo methods, we derive a weighted score matching objective to guide our score-based models to converge correctly to ground states. We first evaluate our approach with experiments on quantum harmonic traps, and results show that it can accurately learn ground states of atomic systems. By implicitly modeling high-dimensional data distributions, our work paves the way toward a more efficient representation of quantum systems.

1 Introduction

Understanding the properties of quantum systems lies at the core of many scientific disciplines, such as condensed matter physics, material science, and quantum chemistry. A quantum system is characterized by its ground state wavefunction, formally obtained by solving the Schrödinger equation. However, directly solving the Schrödinger equation for quantum systems with many particles is impractical due to the exponentially large Hilbert space. Owing to its strong dimension reduction capabilities, deep learning methods have been used as a strong candidate to approximately solve the Schrödinger equation and extract properties of quantum systems with the desired accuracy. For example, under the supervised learning setting, deep learning methods have been successfully applied to predict the quantum properties of molecular systems based on training data generated from density functional theory (DFT) calculation [1–6]. However, supervised methods rely on expensive computational simulations to generate a large amount of training data, and the accuracy of these methods is fundamentally limited by the data quality. Furthermore, DFT calculations involve various approximations and are not guaranteed to reach true ground states. A common scheme for approximately solving the Schrödinger equation is the variational principle, which optimizes a trial

wavefunction to reach the ground state by minimizing its energy as much as possible via quantum Monte Carlo (QMC). Such a method is called variational Monte Carlo, whose accuracy relies on the expressive power of the trial wavefunction. Recently, deep learning methods coupled with variational Monte Carlo have unleashed the potential of both methods [7, 8]. Powered by the efficient sampling and optimization framework of quantum Monte Carlo and the universal approximation capability of deep neural networks, neural wavefunctions can accurately model quantum states, and dramatic improvements have been achieved [9, 10].

Modeling a wavefunction is conceptually similar to modeling a probability density. Existing methods model the wavefunction explicitly by training a neural network to directly output the wavefunction values. However, numerous examples in machine learning have shown that implicitly modeling data distributions provides better representations [11–13]. As our direct reference, score-based methods have demonstrated their strong success in generative modeling [14, 15]. A score is defined as the gradient of the log probability. For example, realistic images can be generated from random noise by following dynamics defined by scores. In this paper, we show that the quantum wavefunction can be represented by score models and be optimized within the QMC framework.

Our motivation to relate score-based models with QMC is based on an interesting connection between energy computations and score-based formulations. In QMC, the energy of a system is averaged over local energy of plausible quantum states. Our observation is that local energy only involves gradients of the logarithmic wavefunction, which we define as the score of the wavefunction. As a result, to minimize energy, the score must be explicitly computed. On the other hand, the actual wavefunction values are only used for sampling and optimization. To this end, we propose a new optimization framework for QMC where sampling and optimization are also achieved by using score functions alone, eliminating the need to explicitly compute the wavefunction value. In our proposed score-based framework, the sampling is done via Langevin dynamics and optimization is done through a new loss function inspired by diffusion Monte Carlo.

Our score-based method enables the possibility of performing QMC computation with only score functions, which is infeasible in existing optimization frameworks. A direct benefit is that, by predicting gradients, we avoid the need to recompute it from the wavefunction. Moreover, score functions can be interpreted as the force of quantum systems, by implicitly modeling distributions with score functions, the dynamics of quantum systems could be better captured. Our experimental results show that with our score-based optimization framework, ground states of quantum systems can be accurately learned.

2 Background and related work

2.1 Quantum many-body wavefunction in continuous space

We use $\mathbf{x} \in \mathbb{R}^{N \times d}$ to denote the coordinates of N particles in d -dimension. The quantum state of a system is defined by its wavefunction $\psi : \mathbb{R}^{N \times d} \rightarrow \mathbb{R}$. By definition ψ is normalized ($\int_{\mathbf{x}} |\psi(\mathbf{x})|^2 = 1$) and $|\psi(\mathbf{x})|^2$ gives the probability density of observing \mathbf{x} . Any wavefunction ψ can be expressed as linear combination of eigenfunctions ψ_n , which are solutions to the time-independent Schrödinger equation $\hat{H}\psi_n(\mathbf{x}) = E_n\psi_n(\mathbf{x})$,

where \hat{H} is a linear operator known as the Hamiltonian, and E_n is a scalar giving the energy of the n -th eigen state. The Hamiltonian is defined as

$$\hat{H}\psi(\mathbf{x}) = -\frac{1}{2} \sum_i \nabla_i^2 \psi(\mathbf{x}) + V(\mathbf{x})\psi(\mathbf{x}), \quad (1)$$

where the index i runs over all of the $N \times d$ dimensions in the summation. The first term in the Hamiltonian takes the sum of the second-order partial derivatives of the wavefunction and is related to the kinetic energy of the system. The second term in the Hamiltonian multiplies the wavefunction by a scalar value and is related to the potential energy of the system. The kinetic term is intrinsic to the Schrödinger equation and always takes the same form, whereas the potential function $V : \mathbb{R}^{N \times d} \rightarrow \mathbb{R}$ varies for different physics problems. Note that although a wavefunction can be complex-valued in general, we can let ψ be real-valued because \hat{H} is real.

Our objective is to find the ground state ψ_0 , which is the eigen state associated with the lowest energy E_0 . In our notation, the coordinates \mathbf{x} can be either viewed as N d -dimensional vectors or as a

flattened $N \cdot d$ dimensional vector. In the rest of this paper, depending on the context, we may use bold \mathbf{x}_i to denote the i -th particle or use the regular font x_i to denote the i -th scalar component of the flattened vector.

2.2 Variational Monte Carlo

The variational Monte Carlo (VMC) method uses a parameterized function $\psi_{\theta} : \mathbb{R}^{N \times d} \rightarrow \mathbb{R}$ (called the Ansatz) to model a wavefunction, where θ denotes the parameters to be optimized. The normalization of ψ_{θ} is not required. The energy expectation of ψ_{θ} is computed as:

$$\mathcal{L}(\theta) = \frac{\int \psi_{\theta}(\mathbf{x}) \hat{H} \psi_{\theta}(\mathbf{x}) d\mathbf{x}}{\int \psi_{\theta}(\mathbf{x}) \psi_{\theta}(\mathbf{x}) d\mathbf{x}} = \frac{\int \psi_{\theta}(\mathbf{x})^2 \frac{\hat{H} \psi_{\theta}(\mathbf{x})}{\psi_{\theta}(\mathbf{x})} d\mathbf{x}}{\int \psi_{\theta}(\mathbf{x})^2 d\mathbf{x}} = \mathbb{E}_{p_{\theta}}[E_L(\mathbf{x}; \theta)], \quad (2)$$

where $E_L(\mathbf{x}; \theta) = \frac{\hat{H} \psi_{\theta}(\mathbf{x})}{\psi_{\theta}(\mathbf{x})}$ is called the *local energy* of \mathbf{x} , $p_{\theta} = \psi_{\theta}^2 / \int \psi_{\theta}^2$ is the probability density. The expectation is evaluated numerically on sparse samples. Markov Chain Monte Carlo (MCMC) sampling is employed to drive sample distribution to converge to the target density p_{θ} .

We can approach ground state wavefunctions by minimizing the energy expectation with gradient descent. The unbiased gradient of $\mathcal{L}(\theta)$ w.r.t. parameters θ is given by:

$$\nabla_{\theta} \mathcal{L}(\theta) = 2 \mathbb{E}_{p_{\theta}}[(E_L(\mathbf{x}; \theta) - \mathbb{E}_{p_{\theta}}[E_L(\mathbf{x}; \theta)]) \nabla_{\theta} \log |\psi_{\theta}(\mathbf{x})|], \quad (3)$$

where expectations are evaluated by average over samples. The derivation of this loss makes use of the fact that \hat{H} is Hermitian [16]. A detailed derivation can be found in Appendix E of Lin et al. [17]. The optimized energy expectation value gives the approximated ground state energy, and the eigenvalue formulation ensures the estimation to be variational, that is, the energy expectation defined by the Ansatz is always above the true ground state energy. Other properties of quantum systems can also be estimated by taking expectations over corresponding operators.

2.3 Related work

Neural quantum state based on the restrictive Boltzmann machine was initially studied for simple quantum spin models on lattices [7]. More complicated neural network architectures, such as convolutional neural network and graph neural network are then extended to more complicated spin systems to capture frustration due to the lattice structure and next nearest neighboring interaction [18, 19]. Similar ideas are also studied for ab-initio simulation in quantum chemistry [20] to study properties of small molecules. Recently, FermiNet [9] and PauliNet [10] greatly improve the accuracy of neural wavefunction and apply to larger molecular systems. Follow-up works contribute to improved performance [21, 22], joint training for multiple geometries [23–25] solving for excited state [26] or for multiple molecules [27, 28]. All of the existing methods use neural networks to explicitly model the wavefunction, while in this work we propose to implicitly model the quantum state using the score function.

Diffusion Monte Carlo (DMC) [29, 30] employs score-based diffusion to improve upon VMC. In VMC, the quality of approximations is limited by the capacity of Ansatz. DMC additionally assigns a weight for each sample in a way that the weighted distribution gives a better approximation of ground state. In DMC’s formulation, each sample is defined by a walker, and each walker is assigned a weight. In importance-sampled DMC, a trial function ψ_T is used. At each iteration, the walkers randomly diffuse by following score of the trial function and the weights are updated according to the imaginary time evolution so that the repeated diffusing and weighting procedure projects out ground states from the trial wavefunction. At convergence, the ground state energy is estimated by the weighted average of local energies. Ceperley and Alder [31] applies DMC to electronic gas. Ren et al. [32] and Wilson et al. [33] apply fixed-node DMC starting from the optimized FermiNet Ansatz.

Score-based methods have shown great success in generative modeling [14, 15]. The effectiveness of implicit density modeling has also been demonstrated by other successful generative models, such as VAEs [11], GANs [12, 34], and diffusion models [35, 13].

3 Method

For the Hamiltonian \hat{H} defined in Equation 1 the local energy can be expressed in terms of the logarithmic wavefunction as:

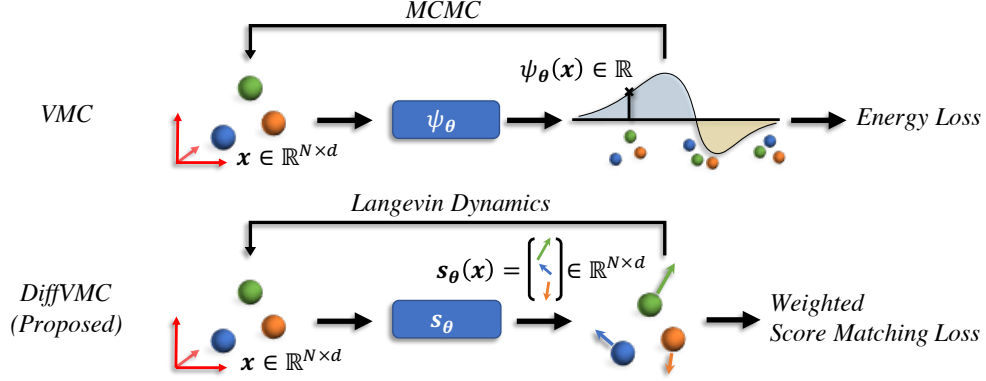


Figure 1: Comparison between the pipeline of VMC and our proposed DiffVMC. In VMC, the wavefunction is explicitly modeled with a neural network, who directly outputs the wavefunction value. The sampling is carried out with MCMC and the optimization is achieved by minimizing the energy loss. In the proposed DiffVMC we instead model the score of the wavefunction. The samples are generated via Langevin dynamics and the proposed weighted score matching objective is employed to optimize the score neural network.

$$E_L(\mathbf{x}; \theta) = -\frac{1}{2} \sum_i \left(\frac{\partial^2 \log |\psi_\theta(\mathbf{x})|}{\partial x_i^2} + \left(\frac{\partial \log |\psi_\theta(\mathbf{x})|}{\partial x_i} \right)^2 \right) + V(\mathbf{x}). \quad (4)$$

One can easily prove this expression by using the fact that $\frac{\partial \log |\psi_\theta(\mathbf{x})|}{\partial x_i} = \frac{1}{x_i} \frac{\partial \psi_\theta(\mathbf{x})}{\partial x_i}$. If we take a closer look at this expression, we can notice that the local energy depends only on the gradient of the logarithmic wavefunction. In fact, if we define the function $\mathbf{s}_\theta : \mathbb{R}^{N \times d} \rightarrow \mathbb{R}^{N \times d}$ such that $\mathbf{s}_\theta(\mathbf{x})_i = \frac{\partial \log |\psi_\theta(\mathbf{x})|}{\partial x_i}$, we can rewrite the local energy as:

$$E_L(\mathbf{x}; \theta) = -\frac{1}{2} (\text{tr}(\nabla_{\mathbf{x}} \mathbf{s}_\theta(\mathbf{x})) + \|\mathbf{s}_\theta(\mathbf{x})\|^2) + V(\mathbf{x}). \quad (5)$$

The function \mathbf{s}_θ is called the *quantum force* or the *drift* in quantum Monte Carlo. Here we follow the convention from the machine learning community and call it the *score*. This direct connection between local energies and scores motivates us to ask the question: can we represent quantum states using only \mathbf{s}_θ ? As a direct benefit, this can avoid recomputing the first-order derivatives in evaluating the local energy and consequently provide a more succinct representation. It is true that we will lose access to the unnormalized wavefunction. However, in practice, our primary goal is to estimate observables, such as kinetic energy or density, which can be estimated from sample distributions.

To this end, our score-based optimization framework follows the gradient descent formulation in VMC, and we design a new loss function inspired by DMC. As we mix the flavors of these two methods, we call our new optimization framework the *Diffusion Variational Monte Carlo* (DiffVMC). The pipelines of VMC and DiffVMC are shown in Figure 1.

Please note that the original score [36] is defined in terms of probability densities, so we have $\mathbf{s}_{\text{original}}(\mathbf{x}) = \nabla_{\mathbf{x}} \log p(\mathbf{x}) = \nabla_{\mathbf{x}} \log \psi(\mathbf{x})^2 = 2 \nabla_{\mathbf{x}} \log |\psi(\mathbf{x})|$, which is twice of the score in our definition. By abuse of notation we define our score in terms of wavefunctions. We do this for two reasons. First, wavefunctions are more natural to deal with in quantum mechanics. Second, as we will show later, in addition to moving samples locally, we also use $\mathbf{s}_\theta(\mathbf{x})$ to describe distributions, which shares the same physical meaning as the original score definition.

3.1 Score-based neural wavefunction ansatz

We use a parameterized score function to implicitly model the wavefunction. Formally, for systems with N particles in d dimension, its score function $\mathbf{s}_\theta : \mathbb{R}^{N \times d} \rightarrow \mathbb{R}^{N \times d}$ maps a set of input coordinates to a set of output scores, which are vectors having the same dimensions as inputs.

Intuitively, after training, the output score should tell the particles the direction toward regions with higher density.

In our case, we are dealing with indistinguishable particles in quantum mechanics. So exchanging two particles will not change the probability density: $\psi(\dots, \mathbf{x}_i, \dots, \mathbf{x}_j, \dots)^2 = \psi(\dots, \mathbf{x}_j, \dots, \mathbf{x}_i, \dots)^2$.

As a result, the score, which is the gradient of a logarithmic wavefunction, is permutation equivariant. Formally,

$$\nabla_{\mathbf{x}_i} \log |\psi(\dots, \mathbf{x}_i, \dots, \mathbf{x}_j, \dots)| = \nabla_{\mathbf{x}_j} \log |\psi(\dots, \mathbf{x}_j, \dots, \mathbf{x}_i, \dots)|. \quad (6)$$

Essentially the equivariance means that if two input particles exchange their positions, their corresponding output score vectors will also exchange positions. The proof is straightforward and we include it in Appendix E. We parameterize the score function with a neural network. The equivariance can be easily achieved by considering the input coordinates as a set [37, 38].

3.2 Sampling via Langevin dynamics

To generate samples that follow the distribution implicitly defined by the score, we use Langevin dynamics, which is similar in the score-based generative models [14]. Given the samples at the current time step \mathbf{x}_t , the coordinates for the new samples are computed as:

$$\mathbf{x}_{t+1} = \mathbf{x}_t + \sqrt{\alpha} \epsilon + \alpha \mathbf{s}_\theta(\mathbf{x}_t), \quad (7)$$

where α is an hyperparameter defining the step size, and $\epsilon \sim \mathcal{N}(\mathbf{0}, \mathbf{I}^{Nd})$ is a random vector sampled from the standard multivariate Gaussian distribution. The process is the same as in DMC and can be understood as first doing a random diffusion, then drifting by following scores. We can prove that when α is small, the distribution converges to the distribution defined by the score function. We empirically validate the theory in Appendix B.

In Langevin dynamics, similar to the Metropolis-Hasting rejection step in MCMC, an accept/reject procedure can be employed to alleviate the finite time error. Although omitted in the context of generative modeling [14], this is a standard step in DMC. The original rejection step computes the ratio

$$P_{\text{acc}} = \frac{\exp\left(-\frac{1}{2\alpha} \|\mathbf{x} - \mathbf{x}' - \mathbf{s}_\theta(\mathbf{x}')\alpha\|^2\right) \psi_\theta(\mathbf{x}')^2}{\exp\left(-\frac{1}{2\alpha} \|\mathbf{x}' - \mathbf{x} - \mathbf{s}_\theta(\mathbf{x})\alpha\|^2\right) \psi_\theta(\mathbf{x})^2}. \quad (8)$$

After each Langevin dynamics move, we decide whether to accept or reject the move based on the P_{acc} . Concretely, we first sample a random number uniformly between 0 and 1. The move is accepted if P_{acc} is larger than the random number and is rejected otherwise. However, the expression of P_{acc} involves the wavefunction values $\psi_\theta(\mathbf{x})$ and $\psi_\theta(\mathbf{x}')$, which are generally not available in our score-based framework. To still be able to use the rejection step, we propose an approximated estimation of P_{acc} which involves only the score function. This is achieved by approximating $\log \frac{|\psi_\theta(\mathbf{x}')|}{|\psi_\theta(\mathbf{x})|} = \log |\psi_\theta(\mathbf{x}')| - \log |\psi_\theta(\mathbf{x})|$ using the average gradient $\frac{1}{2}(\nabla_{\mathbf{x}} \log |\psi_\theta(\mathbf{x})| + \nabla_{\mathbf{x}} \log |\psi_\theta(\mathbf{x}')|)$, then we can show that the ratio can be approximated only in terms of the score as (derivation in Appendix F):

$$P_{\text{acc}} \approx \exp\left(\frac{\alpha}{2} (\|\mathbf{s}_\theta(\mathbf{x})\|^2 - \|\mathbf{s}_\theta(\mathbf{x}')\|^2)\right). \quad (9)$$

3.3 Neural wavefunction optimization

The energy loss in VMC (Equation 3) depends explicitly on wavefunctions. The expression of the energy loss only in terms of scores is unknown. So we need to find a new loss to optimize scores towards ground states. We motivate our new loss from the imaginary time evolution in DMC.

The imaginary time evolution operator $e^{-\tau \hat{H}}$ projects out ground states when $\tau \rightarrow \infty$. At short τ , by Taylor expansion, $e^{-\tau \hat{H}} \psi(\mathbf{x}) \approx \psi(\mathbf{x}) - \tau \hat{H} \psi(\mathbf{x}) = \psi(\mathbf{x}) (1 - \tau \frac{\hat{H} \psi(\mathbf{x})}{\psi(\mathbf{x})}) \approx e^{-\tau E_L(\mathbf{x})} \psi(\mathbf{x})$. Thus, evolving $\psi(\mathbf{x})$ in imaginary time for a short time τ can be approximated as:

$$\psi(\mathbf{x}) \mapsto \psi'(\mathbf{x}) = e^{-\tau E_L(\mathbf{x})} \psi(\mathbf{x}). \quad (10)$$

ψ' is closer to the ground state than ψ because higher energy eigenstates decays exponentially faster than the ground state. Therefore, for our score-based model, we can minimize energies by letting $\mathbf{s}_\theta(\mathbf{x})$ approach the evolved score $\nabla_{\mathbf{x}} \log |\psi'(\mathbf{x})|$. We achieve this via score matching.

Score matching [36] provides a way to make \mathbf{s}_θ converge to the true score of the sample distribution. Assume at current step the samples follow $p = \psi^2 / \int \psi^2$ and $\mathbf{s}_\theta(\mathbf{x}) = \nabla_{\mathbf{x}} \log |\psi(\mathbf{x})|$, we can make $\mathbf{s}_\theta(\mathbf{x})$ converge to $\nabla_{\mathbf{x}} \log |\psi'(\mathbf{x})|$ by minimizing the implicit score matching (ISM) objective:

$$\text{ISM}(\theta) = 2\mathbb{E}_{p'} [\text{tr}(\nabla_{\mathbf{x}} \mathbf{s}_\theta(\mathbf{x})) + \|\mathbf{s}_\theta(\mathbf{x})\|^2], \quad (11)$$

with $p' = \psi'^2 / \int \psi'^2$. The problem is that we do not have samples following p' . We can solve this by transforming the ISM into a weighted version based on current samples:

$$\text{ISM}(\theta) = \frac{2 \int \psi'^2(\mathbf{x}) [\text{tr}(\nabla_{\mathbf{x}} \mathbf{s}_\theta(\mathbf{x})) + \|\mathbf{s}_\theta(\mathbf{x})\|^2] d\mathbf{x}}{\int \psi'^2(\mathbf{x}) d\mathbf{x}} \quad (12)$$

$$= \frac{2 \int \psi^2(\mathbf{x}) e^{-2\tau E_L(\mathbf{x})} [\text{tr}(\nabla_{\mathbf{x}} \mathbf{s}_\theta(\mathbf{x})) + \|\mathbf{s}_\theta(\mathbf{x})\|^2] d\mathbf{x}}{\int \psi^2(\mathbf{x}) d\mathbf{x}} \cdot \frac{\int \psi^2(\mathbf{x}) d\mathbf{x}}{\int \psi'^2(\mathbf{x}) d\mathbf{x}} \quad (13)$$

$$= 2\mathbb{E}_p [e^{-2\tau E_L(\mathbf{x})} [\text{tr}(\nabla_{\mathbf{x}} \mathbf{s}_\theta(\mathbf{x})) + \|\mathbf{s}_\theta(\mathbf{x})\|^2]] \cdot C, \quad (14)$$

where $C = \frac{\int \psi^2(\mathbf{x}) d\mathbf{x}}{\int \psi'^2(\mathbf{x}) d\mathbf{x}} = \frac{\int \psi(\mathbf{x})^2 d\mathbf{x}}{\int \exp(-2\tau E_L(\mathbf{x})) \psi(\mathbf{x})^2 d\mathbf{x}} = (\mathbb{E}_p[\exp(-2\tau E_L(\mathbf{x}))])^{-1}$ is a constant independent of θ . In practice, using small τ makes the loss too small, we thus replace 2τ with a hyperparameter β . We also subtract the sample mean of local energies to improve numerical stability. Put everything together, given a batch of M samples, we define the weighted score matching (WSM) objective as:

$$E_L(\mathbf{x}) = -\frac{1}{2} (\text{tr}(\nabla_{\mathbf{x}} \mathbf{s}_\theta(\mathbf{x})) + \|\mathbf{s}_\theta(\mathbf{x})\|^2) + V(\mathbf{x}) \quad (15)$$

$$E_{\text{diff}}(\mathbf{x}_i) = E_L(\mathbf{x}_i) - \langle E_L \rangle = E_L(\mathbf{x}_i) - \frac{1}{M} \sum_{i=1}^M E_L(\mathbf{x}_i) \quad (16)$$

$$\text{WSM}(\theta) = 2 \sum_{i=1}^M \frac{\exp(-\beta E_{\text{diff}}(\mathbf{x}_i))}{\sum_{i=1}^M \exp(-\beta E_{\text{diff}}(\mathbf{x}_i))} [\text{tr}(\nabla_{\mathbf{x}} \mathbf{s}_\theta(\mathbf{x}_i)) + \|\mathbf{s}_\theta(\mathbf{x}_i)\|^2] \quad (17)$$

$$= 2 \sum_{i=1}^M \underbrace{\sigma(-\beta E_{\text{diff}}(\mathbf{x}_i))_i}_{\text{Does not differentiate w.r.t. } \theta} \underbrace{[\text{tr}(\nabla_{\mathbf{x}} \mathbf{s}_\theta(\mathbf{x}_i)) + \|\mathbf{s}_\theta(\mathbf{x}_i)\|^2]}_{\text{Differentiate w.r.t. } \theta}, \quad (18)$$

where $\sigma(\mathbf{a})_i = \frac{\exp(a_i)}{\sum_i \exp(a_i)}$ is the softmax function. Note that the weighting terms are treated as constant when differentiating the loss w.r.t. the parameters θ . Only the ISM terms require computing gradient during back-propagation. This weighting scheme is similar to the attention mechanism in machine learning where the attention scores are based on the local energies and β plays a similar role to the temperature variable in the Gumbel softmax [39]. As a interesting observation, the ISM (Equation 11) is -4 times the kinetic part in local energy. So we only need to compute one of them and reuse the computation.

We can prove that WSM is unbiased by using the zero-variance property of ground states. At ground states we have $\hat{H}\psi_0(\mathbf{x}) = E_0\psi_0(\mathbf{x})$. Hence $E_L(\mathbf{x}) = \frac{\hat{H}\psi_0(\mathbf{x})}{\psi_0(\mathbf{x})} = E_0$. Consequently, the WSM weights will be identical at ground states and equal to 1 due to softmax. As a result, the WSM loss reduces to the regular ISM loss at the ground state. Moreover, thanks to Langevin dynamics, every state is a local minimum of the ISM loss because the estimated score is the same with the true score of the sample distribution. Hence the ground state is a local minimum of the WSM loss.

Also due to the zero-variance property, when close to ground states, the weights should be close to 1. We can create more imbalanced weights by further normalizing E_{diff} by dividing its standard deviation. We thus have the Scaled-WSM defined as:

$$\text{Scaled-WSM}(\theta) = 2 \sum_{i=1}^M \sigma\left(-\beta \frac{E_{\text{diff}}(\mathbf{x}_i)}{\text{std}(E_{\text{diff}})}\right)_i [\text{tr}(\nabla_{\mathbf{x}} \mathbf{s}_\theta(\mathbf{x}_i)) + \|\mathbf{s}_\theta(\mathbf{x}_i)\|^2]. \quad (19)$$

As in VMC, we update θ according to the loss for one step, then we run Langevin dynamics for several steps to make samples follow the updated score. In our experiments, we use $\beta \sim 1$. So the

Algorithm 1 Diffusion Variational Monte Carlo (DiffVMC)

Input: Randomly initialized sample \mathbf{x} , score network \mathbf{s}_θ , step size α , number of iterations T , number of Langevin dynamics step $N_{\ell d}$

Output: New sample \mathbf{x} , optimized score network \mathbf{s}_θ

```
1: for  $t = 1$  to  $T$  do
2:   for  $i = 1$  to  $N_{\ell d}$  do
3:      $\mathbf{x}' = \mathbf{x} + \sqrt{\alpha}\epsilon + \alpha\mathbf{s}_\theta(\mathbf{x})$ ,  $\epsilon \sim \mathcal{N}(\mathbf{0}, \mathbf{I})$ 
4:      $P_{\text{acc}} = \exp(\frac{\alpha}{2}(\|\mathbf{s}_\theta(\mathbf{x})\|^2 - \|\mathbf{s}_\theta(\mathbf{x}')\|^2))$ 
5:     Sample  $z \sim U(0, 1)$ 
6:     if  $P_{\text{acc}} > z$  then
7:        $\mathbf{x} = \mathbf{x}'$  # Accept the move
8:     end if
9:   end for
10:  loss = Scaled-WSM( $\theta$ )
11:  Update  $\theta$  via gradient descent to minimize the loss.
12: end for
```

short time approximation from imaginary time evolution does not hold strictly. However, since each time we only update parameters for a small step size and that the target wavefunction ψ' is constantly updated, the approximation may still be valid to some extent. But this should be more as an intuition than as a proof. To have further intuition for the convergence behavior, we can compare the WSM loss to the energy gradient 3. In fact, in both cases, we try to increase the probability density for regions with smaller local energies and decrease the probability density for regions with larger local energies. However, by far we do not have a rigorous proof for the convergence property. Nevertheless, in our experiments, systems converge to ground states consistently with the proposed WSM loss.

3.4 The Diffusion Variational Monte Carlo algorithm

The overall procedure is similar to VMC. We first perform several steps of Langevin dynamics to equilibrate the sampling. Then we compute the weighted score matching loss and update the network parameters via gradient descent. The algorithm is summarized in Algorithm 1.

4 Experiments

We first show that our score-based method correctly finds the ground state by solving the harmonic trap. Then we showcase the applicability of our method on simple atomic systems, i.e., interacting fermions with coulomb potential. We will release our code after the review process.

4.1 Wavefunction ansatz for bosons and fermions

Since the unnormalized density $\psi^2(\cdot)$ is invariant under exchange of particle positions (Section 3.1), there are two cases for wavefunction values. The first case is that the wavefunction does not change its sign, i.e., $\psi(\dots, \mathbf{x}_i, \dots, \mathbf{x}_j, \dots) = \psi(\dots, \mathbf{x}_j, \dots, \mathbf{x}_i, \dots)$, such particles are called *bosons*. The second case is that the wavefunction change its sign, i.e., $\psi(\dots, \mathbf{x}_i, \dots, \mathbf{x}_j, \dots) = -\psi(\dots, \mathbf{x}_j, \dots, \mathbf{x}_i, \dots)$, such particles are called *fermions*. These different symmetries will fundamentally change ground states. The fermion ground state must consider the antisymmetric constraint and has higher ground state energy than the boson ground state.

Bosons. We use a feed-forward neural network (Figure 5) composed of multi-layer perceptrons (MLPs) which satisfies the permutation equivariance [37, 38]. Input features are coordinates and distances to the center. Each particle is simultaneously transformed into two feature vectors with two different MLPs. We perform average pooling for the first feature vector over all particles and obtain a global feature. The global feature is then concatenated with the second feature vector. A final MLP is used to predict the score of each particle. All MLPs are shared among different particles.

Fermions. The antisymmetric property of fermions is very challenging to model [40]. Different from bosons, due to the change of sign, the fermion wavefunction has both positive regions and negative regions. The region where the wavefunction equals zero is called the nodal surface (or the node). In

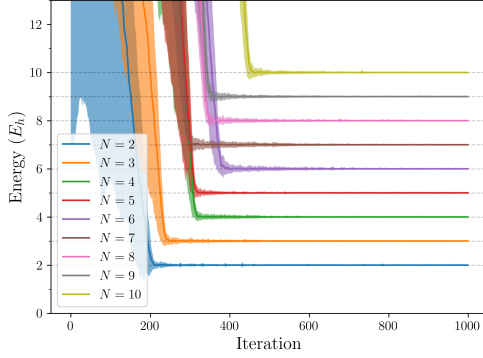


Figure 2: Bosons

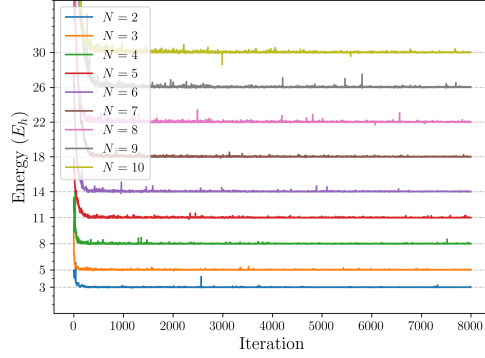


Figure 3: Fermions

Figure 4: Train energies for bosons and fermions in 2d quantum harmonic trap. N is the number of particles. All runs converge correctly to ground states, despite slight fluctuations for fermions.

1-d, the nodal surface is exactly the set where two particles coincide. However, for higher dimension the nodal surface can be arbitrary. The fermion sign structure gives rise some intrinsic difficulties to parametrize the score function. We discuss more on the challenges of fermion antisymmetry in the Appendix H.

Additional difficulty arises from the discontinuity of fermionic scores. In fact, the score function diverges inversely proportionally to the distance away from the nodal surface [41]. Since neural networks essentially models continuous functions, using feed-forward neural networks to model the score function is prohibitive. In fact, even the networks manage to approximately model the discontinuity, in order to compute the local energy we also requires the derivatives of the score to be accurate, which is more difficult.

Wavefunction-based models commonly handle fermion antisymmetries with Slater determinants where input coordinates are encoded into matrices and the wavefunction is given by linear combination of their determinants. As a result, permuting two particles results in permuting two rows in determinants, which will flip the sign of the wavefunction.

Nevertheless, we are still able to illustrate how our score-based framework works with fermions. We can do so by modeling the score as the gradient of an antisymmetric wavefunction Ansatz. We use the score computed from FermiNet [9], where Slater determinants are employed to ensure the antisymmetry. We call it $\nabla_x \text{FermiNet}$. Although by doing so the wavefunction value is practically computed, our goal is to evaluate the our method in this more challenging fermion setting. Currently this stands as the only feasible option to overcome fermion sign problem. More generally we can model scores for fermions as the sum of the gradient of an antisymmetric wavefunction and a symmetric wavefunction:

$$s_{\text{Fermion}}(\mathbf{x}) = \nabla_{\mathbf{x}} f_{\theta_1}(\mathbf{x}) + g_{\theta_2}(\mathbf{x}) - \mathbf{x}. \quad (20)$$

In our setting, f_{θ_1} is FermiNet and we can model g_{θ_2} using a feed-forward network (FFN). In our experiment, FFN uses FermiNet encoder to get a feature vector for each particle, which is then mapped to score via a linear layer. The output of FermiNet score and FFN score are summed together to get the final score. We call it $\nabla_x \text{FermiNet+FFN}$. We do $-\mathbf{x}$ to ensure density vanishes at boundary.

4.2 2D quantum harmonic trap

The Schrödinger equation with harmonic potential

$$V_{\text{QHO}}(\mathbf{x}) = \frac{1}{2} \|\mathbf{x}\|^2. \quad (21)$$

describes a quantum harmonic oscillator, one of the most famous quantum systems that is solvable. The energy levels and eigenstates are known analytically. In particular, for n bosons in the d dimensional harmonic potential, the ground state energy and wavefunction are $E = \frac{nd}{2}$, $|\psi\rangle =$

Table 1: Experimental results on Atoms in Hartree (E_h). Underline denotes our results within chemical accuracy. References taken from Lin et al. [17].

	$\nabla_{\mathbf{x}}\text{FermiNet}$ $\alpha=1\text{e-}3$	$\nabla_{\mathbf{x}}\text{FermiNet}$ $\alpha=1\text{e-}2$	$\nabla_{\mathbf{x}}\text{FermiNet+FFN}$ $\alpha=1\text{e-}3$	FermiNet	HF	Reference
B	-24.64893(22)	<u>-24.65233(3)</u>	-24.63537(46)	-24.65370(3)	-24.53316	-24.65391
C	-37.84414(13)	<u>-37.83445(5)</u>	-37.83736(43)	-37.84471(5)	-37.6938	-37.8450
N	<u>-54.58171(29)</u>	-54.53580(12)	-54.58221(28)	-54.58882(6)	-54.4047	-54.5892
O	<u>-75.06587(63)</u>	-74.94880(709)	-75.06410(53)	-75.06655(7)	-74.8192	-75.0673

$\frac{1}{2^{nd/2}} \exp(-\frac{1}{2}\|\mathbf{x}\|^2)$. Therefore, the quantum harmonic oscillator provides an analytical benchmark for our numerical method. Furthermore, despite its simplicity, the quantum harmonic oscillator is of important experimental relevance and can be realized in cold atom systems by trapping atoms using lasers [42]. Ground states for fermions are more complex due to the antisymmetry constraint. The ground state energies are $E_n = \sum_{i=1}^n e_i$ where $e = 1, 2, 2, 3, 3, 3, 4, \dots$ and the ground state wavefunctions are Slater determinants of Hermite polynomials. We conduct simulation with various number of particles. The results are shown in Figure 4. All runs converge correctly to ground states.

4.3 Atomic systems

For atoms, we work in the Born-Oppenheimer where we assume the atoms are fixed in space and only the electrons are allowed to move. Hence, our inputs are the coordinates of the electrons. The potential due to the Coulomb interactions is:

$$V_{\text{Atom}}(\mathbf{x}) = \sum_{i>j} \frac{1}{\|\mathbf{x}_i - \mathbf{x}_j\|} - \sum_i \frac{Z}{\|\mathbf{x}_i\|}, \quad (22)$$

where Z is the atom charge. As mentioned above, we compute the score by taking the gradient of FermiNet [9]. Following Lin et al. [17], four atoms are tested, including Boron, Carbon, Nitrogen and Oxygen. To show the effect of step size, We trained and tested the score network with $\alpha=1\text{e-}3$ and $\alpha=1\text{e-}2$. We and optimize for 200k iterations for all systems. We use $\beta=2$ for Oxygen and $\beta=1$ for all other atoms. We do Langevin dynamics for 20 steps between two parameter update. The norm of the score is clipped at 20 to increase numerical stability. The complete hyperparameters are in the Appendix G.

The results are summarized on Table 1. The chemical accuracy is defined as 1.594 mE_h [9]. Except for the Nitrogen atom, all atoms can enter the chemical accuracy under one setting, although the effect of step size is mixed. In many cases a higher level of variance is observed. The reason may be due to the difficulty in optimizing the gradient network. Moreover, FermiNet works with the second order optimizer KFAC [43], which is adapted for wavefunction outputs and may not be suitable for our score-based optimization. Nevertheless, our framework has demonstrated the correct convergence behaviour for the challenging electronic potential. The results for N are improved with FFN. For other atoms the results are not improved but are comparable. With this setting we show that in terms of network architectures we can go beyond the FermiNet score.

5 Comparison to VMC and DMC

Compared to DMC, DiffVMC is closer to VMC’s paradigm where Ansatz is optimized by estimating loss based on samples following Ansatz distribution. With DiffVMC we are able to directly model scores, which are more fundamental to the optimization problem and could be more expressive than modeling wavefunctions. On the other hand, DiffVMC and DMC both use scores to update samples. DMC starts with an optimized trial wavefunction Ansatz. Energy minimization is achieved by constantly adjusting weights of walkers. However, the walkers are always guided by the trial function’s score and the parameters of the trial Ansatz cannot be updated in DMC. In contrast, DiffVMC is able to update the guiding score function directly. Nevertheless, there is no conflict between DiffVMC and DMC. DMC walkers can be guided with a score optimized with DiffVMC and further project toward ground state through weighting.

6 Conclusion

Inspired by the connection between the score-based formulation of local energy, we explore the possibility to implicitly model the quantum wavefunction. With the weighted score matching objective, the proposed DiffVMC enables the possibility to optimize the score network toward the ground state. Experiments show that our proposed method can accurately find the ground state for both bosons and fermions.

Acknowledgments

We thank Nicholas Gao for insightful discussions and Cong Fu for providing help on experiments. This work was supported in part by National Science Foundation grants IIS-2006861 and IIS-1908220, and National Institutes of Health grant U01AG070112.

References

- [1] Kristof Schütt, Pieter-Jan Kindermans, Huziel Enoc Saucedo Felix, Stefan Chmiela, Alexandre Tkatchenko, and Klaus-Robert Müller. Schnet: A continuous-filter convolutional neural network for modeling quantum interactions. *Advances in neural information processing systems*, 30, 2017.
- [2] Johannes Gasteiger, Janek Groß, and Stephan Günnemann. Directional message passing for molecular graphs. In *International Conference on Learning Representations (ICLR)*, 2020.
- [3] Yi Liu, Limei Wang, Meng Liu, Yuchao Lin, Xuan Zhang, Bora Oztekin, and Shuiwang Ji. Spherical message passing for 3d molecular graphs. In *International Conference on Learning Representations*, 2022. URL <https://openreview.net/forum?id=givsRXs0t9r>.
- [4] Limei Wang, Yi Liu, Yuchao Lin, Haoran Liu, and Shuiwang Ji. ComENet: Towards complete and efficient message passing for 3D molecular graphs. In *The 36th Annual Conference on Neural Information Processing Systems*, 2022.
- [5] Keqiang Yan, Yi Liu, Yuchao Lin, and Shuiwang Ji. Periodic graph transformers for crystal material property prediction. In *The 36th Annual Conference on Neural Information Processing Systems*, 2022.
- [6] Yuchao Lin, Keqiang Yan, Youzhi Luo, Yi Liu, Xiaoning Qian, and Shuiwang Ji. Efficient approximations of complete interatomic potentials for crystal property prediction. In *International Conference on Machine Learning*, 2023.
- [7] Giuseppe Carleo and Matthias Troyer. Solving the quantum many-body problem with artificial neural networks. *Science*, 355(6325):602–606, 2017.
- [8] Jan Hermann, James Spencer, Kenny Choo, Antonio Mezzacapo, WMC Foulkes, David Pfau, Giuseppe Carleo, and Frank Noé. Ab-initio quantum chemistry with neural-network wavefunctions. *arXiv preprint arXiv:2208.12590*, 2022.
- [9] D. Pfau, J.S. Spencer, A.G. de G. Matthews, and W.M.C. Foulkes. Ab-initio solution of the many-electron schrödinger equation with deep neural networks. *Phys. Rev. Research*, 2:033429, 2020. doi: 10.1103/PhysRevResearch.2.033429. URL <https://link.aps.org/doi/10.1103/PhysRevResearch.2.033429>.
- [10] Jan Hermann, Zeno Schätzle, and Frank Noé. Deep-neural-network solution of the electronic schrödinger equation. *Nature Chemistry*, 12(10):891–897, 2020.
- [11] Diederik P Kingma and Max Welling. Auto-encoding variational bayes. *International Conference on Learning Representations*, 2014.
- [12] Ian J Goodfellow, Jean Pouget-Abadie, Mehdi Mirza, Bing Xu, David Warde-Farley, Sherjil Ozair, Aaron C Courville, and Yoshua Bengio. Generative adversarial nets. In *Advances in Neural Information Processing Systems*, 2014.

- [13] Jonathan Ho, Ajay Jain, and Pieter Abbeel. Denoising diffusion probabilistic models. *Advances in Neural Information Processing Systems*, 33:6840–6851, 2020.
- [14] Yang Song and Stefano Ermon. Generative modeling by estimating gradients of the data distribution. *Advances in Neural Information Processing Systems*, 32, 2019.
- [15] Yang Song, Jascha Sohl-Dickstein, Diederik P Kingma, Abhishek Kumar, Stefano Ermon, and Ben Poole. Score-based generative modeling through stochastic differential equations. In *International Conference on Learning Representations*, 2020.
- [16] David Ceperley, Geoffrey V Chester, and Malvin H Kalos. Monte carlo simulation of a many-fermion study. *Physical Review B*, 16(7):3081, 1977.
- [17] Jeffmin Lin, Gil Goldshlager, and Lin Lin. Explicitly antisymmetrized neural network layers for variational monte carlo simulation. *arXiv preprint arXiv:2112.03491*, 2021.
- [18] Dmitrii Kochkov, Tobias Pfaff, Alvaro Sanchez-Gonzalez, Peter Battaglia, and Bryan K Clark. Learning ground states of quantum hamiltonians with graph networks. *arXiv preprint arXiv:2110.06390*, 2021.
- [19] Cong Fu, Xuan Zhang, Huixin Zhang, Hongyi Ling, Shenglong Xu, and Shuiwang Ji. Lattice convolutional networks for learning ground states of quantum many-body systems. *arXiv preprint arXiv:2206.07370*, 2022.
- [20] Jiequn Han, Linfeng Zhang, and E Weinan. Solving many-electron schrödinger equation using deep neural networks. *Journal of Computational Physics*, 399:108929, 2019.
- [21] Leon Gerard, Michael Scherbela, Philipp Marquetand, and Philipp Grohs. Gold-standard solutions to the schrödinger equation using deep learning: How much physics do we need? *arXiv preprint arXiv:2205.09438*, 2022.
- [22] Ingrid von Glehn, James S Spencer, and David Pfau. A self-attention ansatz for ab-initio quantum chemistry. *arXiv preprint arXiv:2211.13672*, 2022.
- [23] Nicholas Gao and Stephan Günnemann. Ab-initio potential energy surfaces by pairing gnns with neural wave functions. In *International Conference on Learning Representations*, 2021.
- [24] Michael Scherbela, Rafael Reisenhofer, Leon Gerard, Philipp Marquetand, and Philipp Grohs. Solving the electronic schrödinger equation for multiple nuclear geometries with weight-sharing deep neural networks. *Nature Computational Science*, 2(5):331–341, 2022.
- [25] Nicholas Gao and Stephan Günnemann. Sampling-free inference for ab-initio potential energy surface networks. *arXiv preprint arXiv:2205.14962*, 2022.
- [26] Mike Entwistle, Zeno Schätzle, Paolo A Erdman, Jan Hermann, and Frank Noé. Electronic excited states in deep variational monte carlo. *arXiv preprint arXiv:2203.09472*, 2022.
- [27] Nicholas Gao and Stephan Günnemann. Generalizing neural wave functions. *arXiv preprint arXiv:2302.04168*, 2023.
- [28] Michael Scherbela, Leon Gerard, and Philipp Grohs. Towards a foundation model for neural network wavefunctions. *arXiv preprint arXiv:2303.09949*, 2023.
- [29] Julien Toulouse, Roland Assaraf, and Cyrus J Umrigar. Introduction to the variational and diffusion monte carlo methods. In *Advances in Quantum Chemistry*, volume 73, pages 285–314. Elsevier, 2016.
- [30] David M Ceperley. Introduction to quantum monte carlo methods applied to the electron gas. In *The Electron Liquid Paradigm in Condensed Matter Physics*, pages 3–42. IOS Press, 2004.
- [31] David M Ceperley and Berni J Alder. Ground state of the electron gas by a stochastic method. *Physical review letters*, 45(7):566, 1980.
- [32] Weiluo Ren, Weizhong Fu, and Ji Chen. Towards the ground state of molecules via diffusion monte carlo on neural networks. *arXiv preprint arXiv:2204.13903*, 2022.

- [33] Max Wilson, Nicholas Gao, Filip Wudarski, Eleanor Rieffel, and Norm M Tubman. Simulations of state-of-the-art fermionic neural network wave functions with diffusion monte carlo. *arXiv preprint arXiv:2103.12570*, 2021.
- [34] Andrew Brock, Jeff Donahue, and Karen Simonyan. Large scale gan training for high fidelity natural image synthesis. *arXiv preprint arXiv:1809.11096*, 2018.
- [35] Jascha Sohl-Dickstein, Eric Weiss, Niru Maheswaranathan, and Surya Ganguli. Deep unsupervised learning using nonequilibrium thermodynamics. In *International Conference on Machine Learning*, pages 2256–2265. PMLR, 2015.
- [36] Aapo Hyvärinen and Peter Dayan. Estimation of non-normalized statistical models by score matching. *Journal of Machine Learning Research*, 6(4), 2005.
- [37] Manzil Zaheer, Satwik Kottur, Siamak Ravanbakhsh, Barnabas Poczos, Russ R Salakhutdinov, and Alexander J Smola. Deep sets. *Advances in neural information processing systems*, 30, 2017.
- [38] Charles R Qi, Hao Su, Kaichun Mo, and Leonidas J Guibas. Pointnet: Deep learning on point sets for 3d classification and segmentation. In *Proceedings of the IEEE conference on computer vision and pattern recognition*, pages 652–660, 2017.
- [39] Eric Jang, Shixiang Gu, and Ben Poole. Categorical reparameterization with gumbel-softmax. *arXiv preprint arXiv:1611.01144*, 2016.
- [40] David M Ceperley. Fermion nodes. *Journal of statistical physics*, 63(5):1237–1267, 1991.
- [41] CJ Umrigar, MP Nightingale, and KJ Runge. A diffusion monte carlo algorithm with very small time-step errors. *The Journal of chemical physics*, 99(4):2865–2890, 1993.
- [42] Franco Dalfovo, Stefano Giorgini, Lev P Pitaevskii, and Sandro Stringari. Theory of bose-einstein condensation in trapped gases. *Reviews of modern physics*, 71(3):463, 1999.
- [43] James Martens and Roger Grosse. Optimizing neural networks with kronecker-factored approximate curvature. In *International conference on machine learning*, pages 2408–2417. PMLR, 2015.
- [44] Tianyu Pang, Kun Xu, Chongxuan Li, Yang Song, Stefano Ermon, and Jun Zhu. Efficient learning of generative models via finite-difference score matching. *Advances in Neural Information Processing Systems*, 33:19175–19188, 2020.
- [45] Adam Paszke, Sam Gross, Soumith Chintala, Gregory Chanan, Edward Yang, Zachary DeVito, Zeming Lin, Alban Desmaison, Luca Antiga, and Adam Lerer. Automatic differentiation in pytorch. In *31st Conference on Neural Information Processing Systems*, 2017.
- [46] James Bradbury, Roy Frostig, Peter Hawkins, Matthew James Johnson, Chris Leary, Dougal Maclaurin, George Necula, Adam Paszke, Jake VanderPlas, Skye Wanderman-Milne, and Qiao Zhang. JAX: composable transformations of Python+NumPy programs, 2018. URL <http://github.com/google/jax>.
- [47] David Pfau James S. Spencer and FermiNet Contributors. FermiNet, 2020. URL <http://github.com/deepmind/ferminet>.

A Limitation

Although predicting score could in principle lead to a more expressive neural wavefunction model, as indicated by the ∇_x FermiNet+FFN architecture, the optimization for fermion systems remains a challenge. In fact, current deep VMC methods rely on second-order optimization methods. This is primarily due to the singularities of local energy near the nodal surfaces, which are induced by the fermion antisymmetry. However, current optimization methods (e.g., KFAC [43]) require knowing the explicit wavefunction and thus not completely suitable for score-based models. In this work, we aim to demonstrate the feasibility of such a score-based framework where ground states of quantum many-body systems can be accurately achieved by using the proposed sampling method and optimizing the proposed loss function. The development of an effective optimization method for the score-based formulation remains to be studied in future work.

B Langevin dynamics sampling

In this section we analyse the accuracy of Langevin dynamics sampling. We first train a FermiNet on the Nitrogen atom using the conventional MCMC sampling with Metropolis-Hasting (MH) rejection. Then we generate samples with MCMC or with Langevin dynamics. For the latter we investigate the effect of varying step sizes and different rejection methods. We use 512 walkers for all Langevin dynamics evaluations, and samples are gathered from 20,000 steps, with 20 decorrelation steps interspersed. The average acceptance probability \bar{p}_{move} as well as the average and median of sample energies are reported. The results show that when our approximated MH rejection is used, the evaluated mean energy is stable and is close to the energy obtained by MCMC (well within chemical accuracy). However, when no rejection is performed, the evaluated energies become unstable. In fact, even without the rejection step, most sampled energies are close to the ground state energy, as shown by the median of energies. However, without rejection steps, walkers could accidentally move too close to the fermion nodes (regions with zero wavefunction values), where the local energy diverges, thereby introduce huge variance in the mean energy. Nevertheless, our analysis shows that with the approximated rejection step, sampling with Langevin dynamics remains sufficiently reliable to estimate energies, at least for small systems.

Table 2: Analysis of Langevin dynamics sampling. The standard deviation of the last digits of energies are indicated in parentheses. For rejection methods, “Approx” means moves are rejected or kept using our proposed approximated rejection ratio (Equation 9) and “None” means no rejection step is performed.

Sampling	Rejection	Step size α	\bar{p}_{move}	Energy mean	Energy median
MCMC	MH	-	0.5382	-54.58921(6)	-54.58704
Langevin dynamics	Approx	1e-4	0.9998	-54.58917(12)	-54.58693
Langevin dynamics	Approx	1e-3	0.9978	-54.58914(6)	-54.58710
Langevin dynamics	Approx	1e-2	0.9626	-54.58889(4)	-54.58693
Langevin dynamics	None	1e-4	1	-54.83(15)	-54.58719
Langevin dynamics	None	1e-3	1	-54.96 (69)	-54.58706
Langevin dynamics	None	1e-2	1	-108 (47)	-54.58695

C Problem with stochastic gradients

In this section we discuss the reason why we cannot use the sample mean of local energies as loss function but instead need a specially designed loss. We can write the local energy at \mathbf{x}_i as $E_L(\mathbf{x}_i, \boldsymbol{\theta}) = E_k(\mathbf{x}_i, \boldsymbol{\theta}) + V(\mathbf{x}_i)$, where E_k is the kinetic energy and V is the potential energy. Note that only $E_k(\mathbf{x}_i, \boldsymbol{\theta})$ depends on parameters $\boldsymbol{\theta}$ whereas $V(\mathbf{x}_i)$ only depends on the positions \mathbf{x}_i and is independent of the wavefunction or $\boldsymbol{\theta}$. Therefore, if we use the sample mean of local energies as loss function, then the parameter updates will be independent of potential V . Moreover, since Langevin dynamic (or MCMC) does not involve V neither, the entire optimization process will be independent of V , which will make optimization fail.

Also, having noticed the connection between kinetic energy and score matching objective, we can have another interpretation from score matching. As discussed above, since $V(\mathbf{x}_i)$ depends on θ , optimizing $\hat{\mathcal{L}}(\theta)$ is equivalent to optimizing $\frac{1}{N} \sum_i E_k(\mathbf{x}_i, \theta)$, which according to our observation, is equal to $-\frac{1}{4} \frac{1}{N} \sum_i ISM(\mathbf{x}_i, \theta)$, where ISM is the implicit score matching objective. So intuitively, optimizing $\hat{\mathcal{L}}(\theta)$ is equivalent to optimizing the score matching objective in the opposite direction, which will make the learned score (or wavefunction) away from sample distribution. On the other hand, Langevin dynamics (or MCMC) will make sample distribution close to the learned score (or wavefunction). As a result, the optimization process will never attain equilibrium.

D Computational complexity

Compared to VMC, DiffVMC avoids recomputing gradient of wavefunctions during energy evaluation, but the loss is more complicated. So the overall computational cost is similar with VMC. In our experiments with FermiNet, DiffVMC is slower than VMC because we need to backpropagate through the gradient network. This could potentially be mitigated with more adapted network architectures. In general, the major computation bottleneck of QMC is evaluating $\text{tr}(\nabla_{\mathbf{x}} \mathbf{s}(\mathbf{x}))$ which cannot be paralleled efficiently. The evaluation and backpropagation of our ISM loss have similar computational cost with evaluating the local energy. Fortunately, since ISM loss has similar formula with the kinetic energy, we can reuse the computations to mitigate these costs. Further, by noticing the connection between kinetic energy and score matching, we might be able to accelerate this computation via more efficient score matching techniques [14, 15, 44] in future work.

E Proof for equivariance

We show it for two 1-d particles:

$$\partial_1 \log |\psi(x_1, x_2)| = \lim_{\Delta x \rightarrow 0} \frac{\log |\psi(x_1 + \Delta x, x_2)| - \log |\psi(x_1, x_2)|}{\Delta x} \quad (23)$$

$$= \lim_{\Delta x \rightarrow 0} \frac{\log |\psi(x_2, x_1 + \Delta x)| - \log |\psi(x_2, x_1)|}{\Delta x} = \partial_2 \log |\psi(x_2, x_1)|. \quad (24)$$

F Derivation of the approximated detailed balancing

The original detailed balancing in Langevin Monte Carlo is

$$P_{\text{acc}}(\mathbf{x}'|\mathbf{x}) = \frac{\exp\left(-\frac{1}{2\alpha} \|\mathbf{x} - \mathbf{x}' - \mathbf{s}_{\theta}(\mathbf{x}')\alpha\|^2\right) \psi_{\theta}(\mathbf{x}')^2}{\exp\left(-\frac{1}{2\alpha} \|\mathbf{x}' - \mathbf{x} - \mathbf{s}_{\theta}(\mathbf{x})\alpha\|^2\right) \psi_{\theta}(\mathbf{x})^2} \quad (25)$$

In our score-based framework, we generally do not have access to wavefunction value. So our goal here is to get rid of the explicit dependencies on $\psi_{\theta}(\mathbf{x}')$ and $\psi_{\theta}(\mathbf{x})$. We can do so by assuming the score is constant between \mathbf{x} and \mathbf{x}' . We first transform into the log domain:

$$\log P_{\text{acc}} = -\frac{1}{2\alpha} \underbrace{(\|\mathbf{x} - \mathbf{x}' - \mathbf{s}_{\theta}(\mathbf{x}')\alpha\|^2 - \|\mathbf{x}' - \mathbf{x} - \mathbf{s}_{\theta}(\mathbf{x})\alpha\|^2)}_A + 2 \underbrace{(\log |\psi_{\theta}(\mathbf{x}')| - \log |\psi_{\theta}(\mathbf{x})|)}_B \quad (26)$$

where we use A and B to denote the two components and $\log P_{\text{acc}} = A + B$.

We first simplify A . By expanding the norms as $\|\mathbf{x} - \mathbf{x}' - \mathbf{s}_{\theta}(\mathbf{x}')\alpha\|^2 = \|\mathbf{x} - \mathbf{x}'\|^2 - 2\langle \mathbf{x} - \mathbf{x}', \mathbf{s}_{\theta}(\mathbf{x}') \rangle \alpha + \|\mathbf{s}_{\theta}(\mathbf{x}')\|^2 \alpha^2$ and $\|\mathbf{x}' - \mathbf{x} - \mathbf{s}_{\theta}(\mathbf{x})\alpha\|^2 = \|\mathbf{x}' - \mathbf{x}\|^2 - 2\langle \mathbf{x}' - \mathbf{x}, \mathbf{s}_{\theta}(\mathbf{x}) \rangle \alpha + \|\mathbf{s}_{\theta}(\mathbf{x})\|^2 \alpha^2$, we obtain:

$$A = \langle \mathbf{x} - \mathbf{x}', \mathbf{s}_{\theta}(\mathbf{x}') + \mathbf{s}_{\theta}(\mathbf{x}) \rangle + \frac{\alpha}{2} (\|\mathbf{s}_{\theta}(\mathbf{x})\|^2 - \|\mathbf{s}_{\theta}(\mathbf{x}')\|^2) \quad (27)$$

To simplify B , we use the approximation:

$$\log |\psi_{\theta}(\mathbf{x}')| - \log |\psi_{\theta}(\mathbf{x})| \approx \left\langle \frac{1}{2} (\nabla_{\mathbf{x}} \log |\psi_{\theta}(\mathbf{x}')| + \nabla_{\mathbf{x}} \log |\psi_{\theta}(\mathbf{x})|), \mathbf{x}' - \mathbf{x} \right\rangle \quad (28)$$

$$= \frac{1}{2} \langle \mathbf{s}_{\theta}(\mathbf{x}') + \mathbf{s}_{\theta}(\mathbf{x}), \mathbf{x}' - \mathbf{x} \rangle \quad (29)$$

Such approximation is commonly employed in finite difference methods. The approximation is valid since \mathbf{x} and \mathbf{x}' are close in space. With this approximation, we have:

$$B = 2(\log |\psi_{\theta}(\mathbf{x}')| - \log |\psi_{\theta}(\mathbf{x})|) \approx -\langle \mathbf{x} - \mathbf{x}', \mathbf{s}_{\theta}(\mathbf{x}') + \mathbf{s}_{\theta}(\mathbf{x}) \rangle \quad (30)$$

Finally,

$$\log P_{\text{acc}} = A + B \approx \frac{\alpha}{2} (\|\mathbf{s}_{\theta}(\mathbf{x})\|^2 - \|\mathbf{s}_{\theta}(\mathbf{x}')\|^2) \quad (31)$$

G Computational settings

We implement DiffVMC in Pytorch [45] for experiments with Bosons and in Jax [46] for experiments with Fermions. All gradient computation is done with automatic differentiation from the respective libraries. For experiments with FermiNet, we adapt based on the official implementation of FermiNet [47]. The hyperparameters for training are summarized in Table 3 and Table 4. For evaluation, we first anneal the the MCMC chain for 1000 steps. Then we execute Langevin dynamics and gather samples from 20,000 different steps, with 20 MCMC steps being run between two consecutive collections.

Table 3: Hyperparameters for Bosons

Network	Hidden dim	32
	# MLP layers	3
Optimization	Optimizer	Adam
	Batch size	256
	Learning rate	5e-4
	Optimization steps	2000
	Clip local energy	$5 \times \text{std}$
	WSM - β	1
Langevin dynamics	Langevin dynamics steps	20
	Metroplis Hasting rejection	Approximate (Equation 9)
	Step size α	0.01
	Score norm clip	20

Table 4: Hyperparameters for Fermions

FermiNet	# determinants	16 (for atoms) or 1 (for QHO)
	Single layer hidden dim	256
	Double layer hidden dim	32
	# embedding layers	4
Side network (FFN)	Single layer hidden dim	64
	Double layer hidden dim	8
	# embedding layers	4
Optimization	Pertraining steps	500 (for B, C) or 1000 (for N, O)
	Batch size	256 (for B, C) or 512 (for N, O)
	Optimizer	Kfac
	Kfac - damping	0.001
	Kfac - norm constraint	0.001
	Initial learning rate	5e-2
	Learning rate decay	$\text{lr}_{\text{init}} \times (1 + t/10000)^{-1}$
	Clip local energy	$5 \times \text{std}$
	WSM - β	1 or 2
Langevin dynamics	Langevin dynamics steps	20
	Metroplis Hasting rejection	Approximate (Equation 9)
	Step size α	0.001 or 0.01
	Optimization steps	200,000
	Score norm clip	20

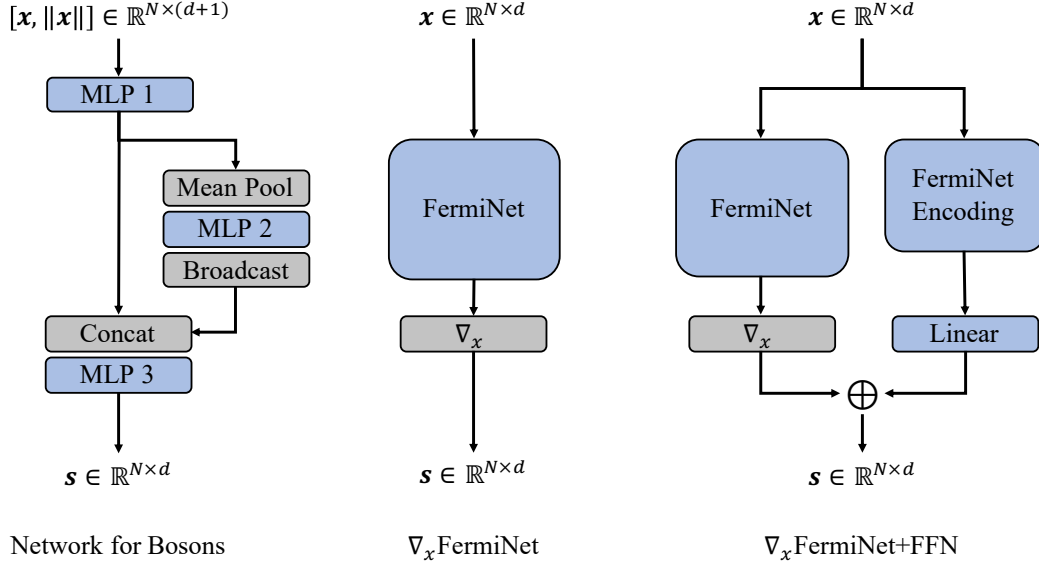


Figure 5: Network architectures. MLPs are composed with 3 linear layers interleaved with 2 SiLU activations. $-x$ is omitted in ∇_x FermiNet+FFN for simplicity. ∇_x means computing derivatives of network outputs with respect to input coordinates.

H Challenges of fermion antisymmetry

To show the challenges of fermion antisymmetry, We discuss some examples where we try to use pure score functions to learn ground states for fermions in QHO potentials.

In 1D, fermion wavefunctions become zero exactly when any two particles coincide in space. To handle such antisymmetric constraint, we can let scores diverge at such configurations. To be concrete, the score for the i -th particle is defined as $s_\theta(x_i, |x_1, \dots, x_N) = \text{FFN}(x_i | x_1, \dots, x_N) + \sum_{j \neq i} \frac{1}{x_i - x_j}$,

where FFN is a feedforward network with the same architecture used for the Bosons. The second term in the right hand side ensures the score to diverge when any two particles are close. The results are shown in Figure 6.

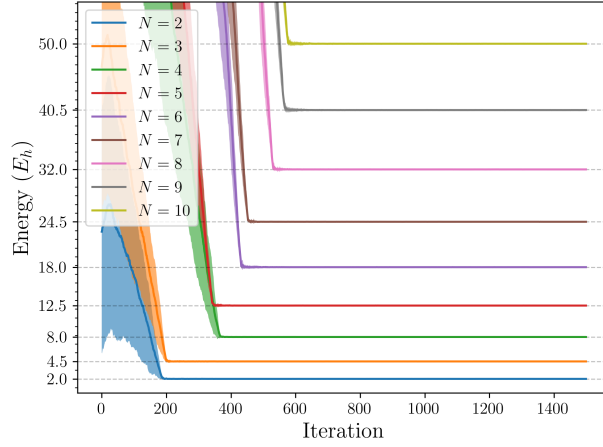


Figure 6: Fermions in 1-dimensional QHO potential with pure score functions. N denotes the number of particles.

The single-particle energy levels are $n + \frac{1}{2}$, $n = 0, 1, 2, \dots$. Hence by Pauli exclusion, the ground states energies for 2 and more particles are 2, 4.5, 8, 12.5, etc. We can see that this works correctly for the 1D case. However, this is not surprising because the ground truth scores function for 1D QHO are in the form of $s_{\text{gt}}(x_i|x_1, \dots, x_N) = -x_i + \sum \frac{1}{x_i - x_j}$. As a result, the learning is not difficult as long as the optimization is correct. We show the sample distributions for 2 particles in Figure 7, the antisymmetric w.r.t. to $x_1 = x_2$ is correctly captured.

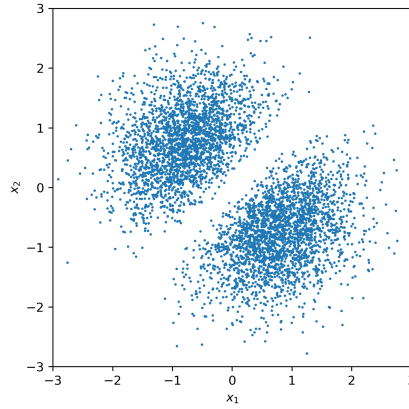


Figure 7: Sample distribution for two 1-dimensional particles in a QHO potential with 5000 samples. X and Y axes give the positions of the first and the second particles, respectively.

This however does not extend to more than 1D. The results for the 2D case with the same network is shown in Figure 8. The 2D single-particle energy levels are 1, 2, 2, 3, 3, 3, 4, 4, 4, 4, ... (note degenerencies in energy levels). So the ground states energies for 2 and more particles should be 3, 5, 8, 11, 14, etc, as correctly predicted in Figure 2(b) of our paper. However, the prediction with the pure score function gives 4, 9, 16, 25, 36, etc. So this simple network fails to capture the 2-dimensional fermion nodes and constraints are too restrictive. With more sophisticated network designs or training strategies we are able to get correct energies for 2 particles, but still fail for more general cases. In fact, fermion nodal surfaces for 2 or higher dimensions can be arbitrary and can occur without contact between particles. For example, as depicted in Figure 9, two fermions can exchange their positions with a 180-degree rotation around their center. The wavefunction will change sign before

and after the rotation so the wavefunction must be zero at least once during the rotation, however, the distance between two particles do not change. To conclude, designing antisymmetric score functions without using gradients of determinants is highly non-trivial and may require further theoretical investigations.

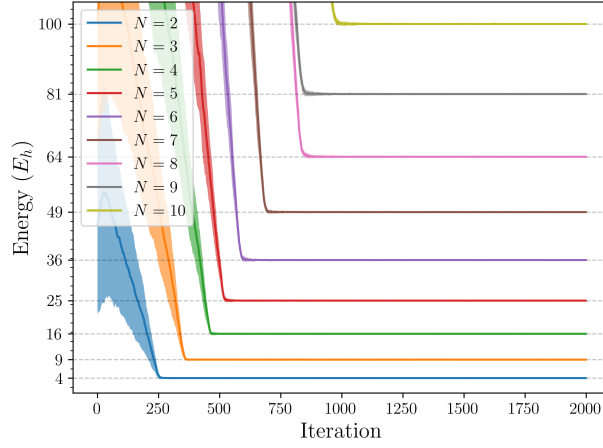


Figure 8: Failure case: Fermions in a 2-dimensional QHO potential with pure score functions. N denotes the number of particles.

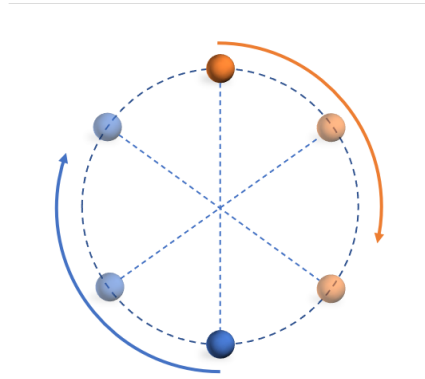


Figure 9: 2 2-dimensional Fermions exchange positions with a 180-degree rotation around the center.